CHAPTER - 3

EN AW6082 METAL MATRIX COMPOSITES REINFORCED WITH GARNET PARTICLES

Chapter - 3

EN AW6082 METAL MATRIX COMPOSITES REINFORCED WITH GARNET PARTICLES*

The 6xxx series of Al-Mg-Si alloys have a wide range of industrial applications due to their excellent mechanical properties, good joining ability, corrosion resistance, low density, and good workability. Therefore, these alloys are considered as suitable material for structural applications. On the other hand, garnet, an industrial by-product of the rare earth oxide extraction from beach sand, has been found to be one of the potential reinforcement options. As garnet is cheap, abundantly available and has a Moh's hardness of 6.5 to 7.0, which is nearly equal to that of SiC, it can be used as a suitable reinforcement for Al matrix composite. In spite of the available literature on corrosion resistance and sliding wear behavior of garnet particulate-reinforced Al alloys [Seah *et al*. (2001) and Sharma (2001)], the effect of garnet on the structural/morphological behavior and mechanical properties of aluminum alloys as well as nanocomposite powders is not yet fully understood. Therefore, the present investigation aims at studying the effect of milling time, role of alloying elements and dispersion of garnet particulates on the structure, morphology, and mechanical properties of commercial aluminum and EN AW6082 Al-Si-Mg alloy composite powders produced by high-energy ball milling.

---

* A part of this work is published in *Metallurgical and Materials Transactions: A* **46**, 1360-1373 (2015).

In the present study, the morphology, structure and hardness variations of garnet reinforced EN AW 6082 Aluminum alloy composites have been investigated. High-energy ball milling of EN AW6082 Al-alloy powder, with and without garnet reinforcement, was performed under argon atmosphere for various durations up to 50 hour. The study aimed at exploring the role of alloying elements and hard reinforcement particles on the structural evolution at different stages of mechanical milling. The composite powders were characterized in terms of the morphological variation, microstructural evolution, and thermal stability. Conventional microindentation and nanoindentation measurements were carried out on the individual powders as well as composite particles to estimate the changes in the mechanical properties of the composites with milling time.

3.1 Structural evolution during milling

The typical XRD patterns of EN AW6082, EN AW6082/Garnet, and Al/Garnet powder mixtures at different stages of MM are shown in Figs. 3.1, 3.2 and 3.3. These patterns exhibit distinct major peaks corresponding to face centered cubic α-Al and weak diffraction peaks of garnet. For unreinforced EN AW6082, peaks related to alloying elements disappeared completely after 10 hours of milling, as shown in Fig. 3.1. The absence of Si and Mg containing intermetallic peaks may be attributed to the gradual dissolution of these minor alloying elements into the α-Al matrix with increasing milling time. Similar results were observed by other researchers as well [Deaquino-Lara *et al.* (2011) and Sivasankaran *et al.* (2010)]. During continuous milling, α-Al peaks decreased in intensity and simultaneously peak width increased with the increase of milling time, denoting a microstructural refinement. During high

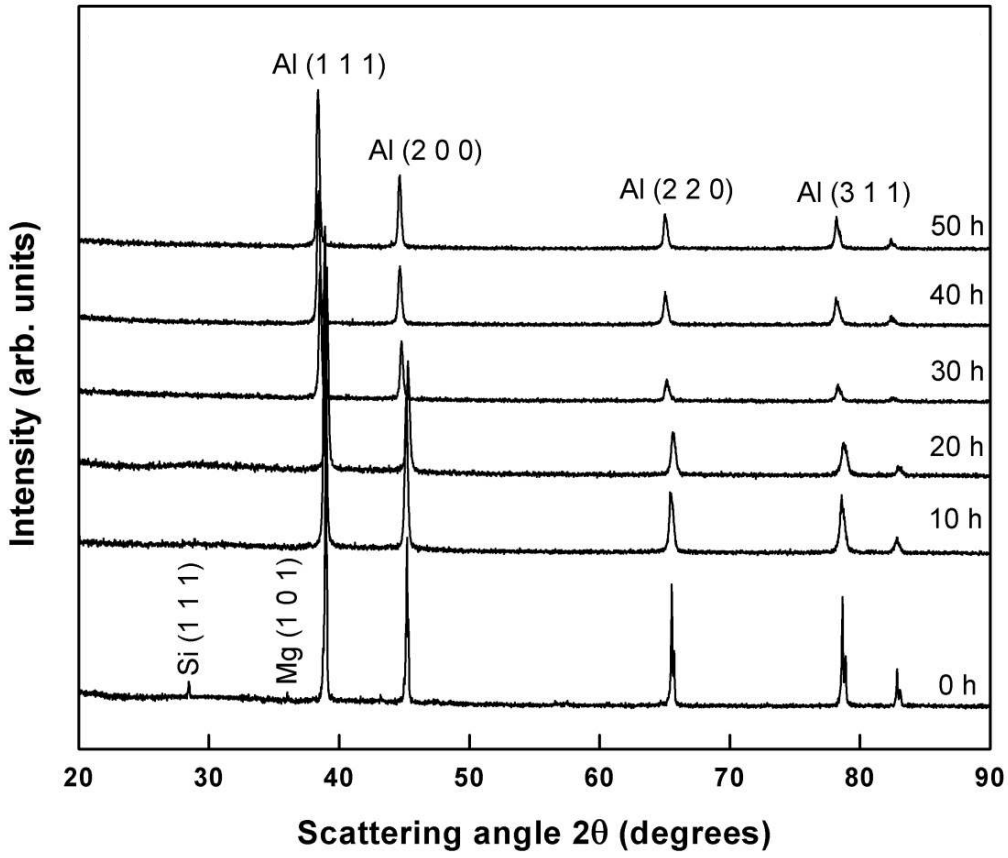

Figure 3.1: XRD patterns of unreinforced EN AW6082 powder after 10, 20, 30, 40, and 50 h of high-energy ball milling.

ball milling, the powders experience repeated collision, fracture, and cold welding. The severe plastic deformation induced by the above processes lead to grain refinement, accumulation of internal stresses that changes the lattice parameter and formation of cell structure [Suryanarayana (2001), Ares *et al*. (2005) and Delshad Chermahinia *et al*. (2009)]. Along with the cold welding event during high-energy ball milling, some powders also coat the grinding medium and/or the inner walls of the container. A thin

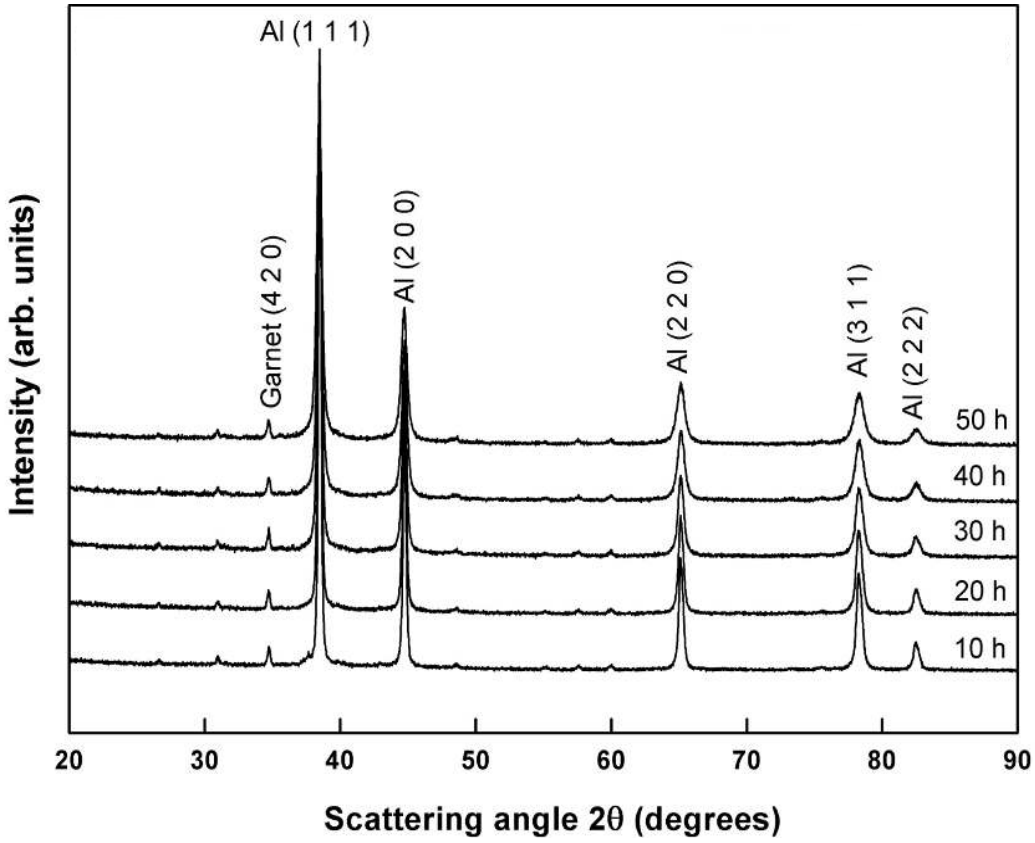

Figure 3.2: XRD patterns of EN AW6082/Garnet composite powder after 10, 20, 30, 40, and 50 h of high-energy ball milling.

layer of the coating is thus beneficial in preventing wear and tear of the grinding medium and also in preventing contamination of the milled powder with the debris. However, the level of contamination is very low, so the Fe peaks was not observed and can be attributed to the limitation of the filtered X-ray to detect phases with amount less than 2.0 wt.%. Also, the XRD pattern of the milled powders evidenced that no intermetallic peak was formed and the material obtained did consist of only Al phase without any secondary phase even after 50 hours of milling. The sharp crystalline peaks (Figs. 3.2 and 3.3) broadened progressively with increasing milling time and refinement

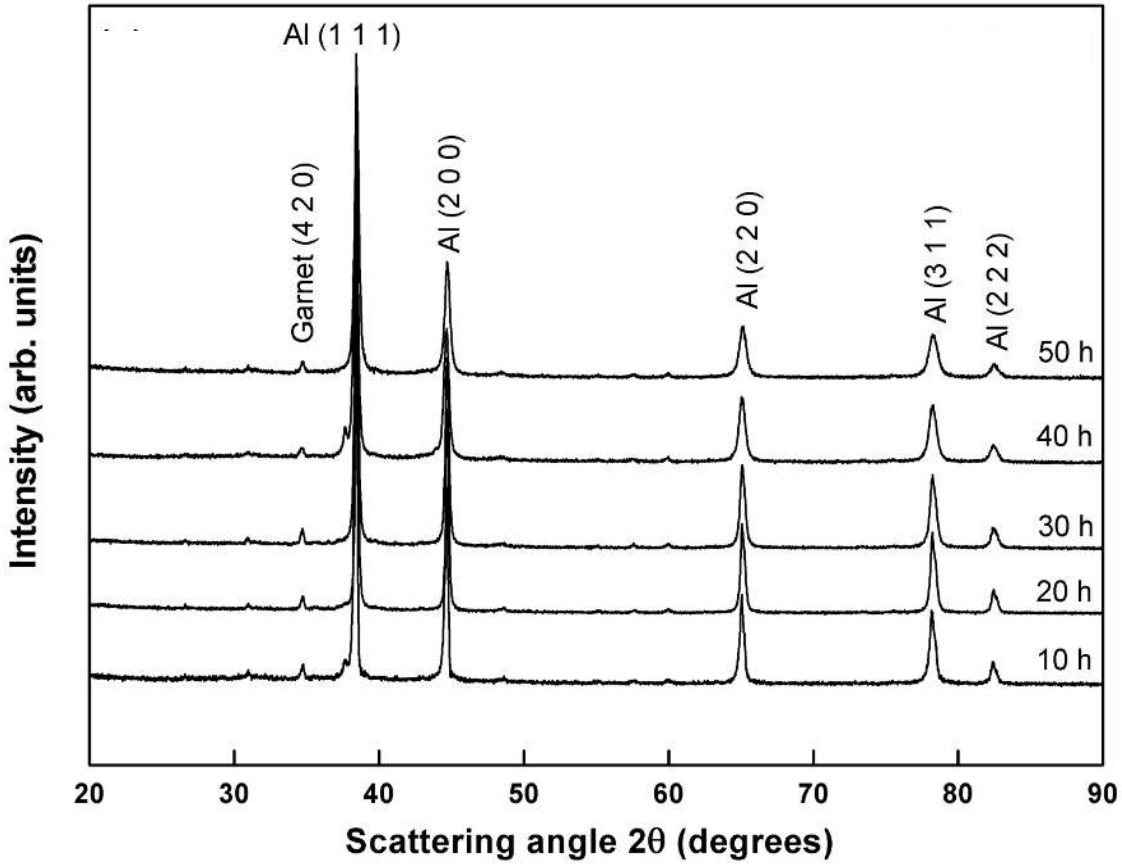

Figure 3.3: XRD patterns of Al/Garnet composite powder after 10, 20, 30, 40, and 50 h of high-energy ball milling.

of grain size down to nanometer range, in both aluminum and EN AW6082, was observed. The reduction in crystallite size was due to the creation of a large numbers of linear defects, particularly dislocations, which resulted in formation of sub-cells [Razavi *et al*. (2009)]. Figs. 3.4 and 3.5 show the position (i.e., 2h diffraction angles) of the first intense peak Al (111) from all the milling durations. In unreinforced EN AW6082, the peak positions shift towards lower values of diffraction angle and then to higher values as the milling time increases. The displacement of Al (111) peak towards lower angles,

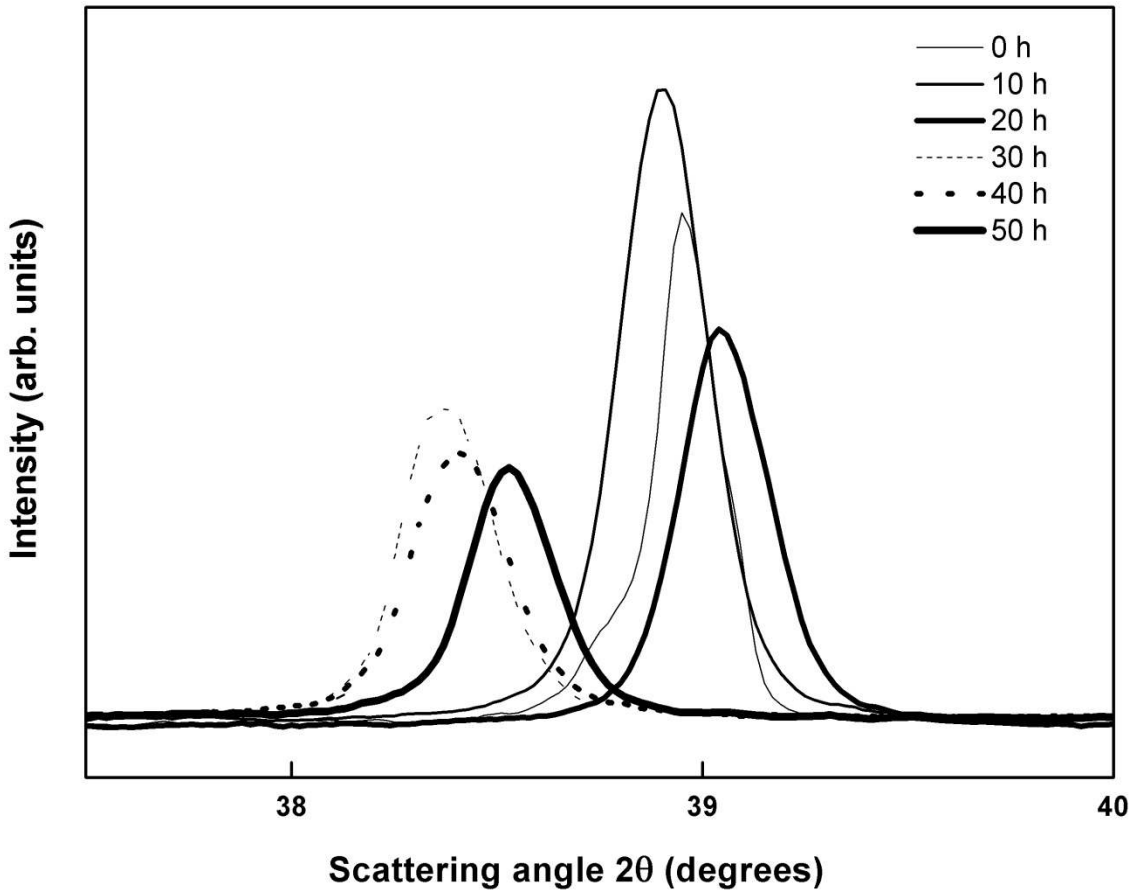

Figure 3.4: Evolution of d_{111} peak intensity on powder XRD showing the broadening and reduction in intensity milled at different hours for unreinforced EN AW6082.

which in turn indicates increase in Al lattice parameter, with increasing milling time suggests the gradual dissolution of alloying elements, namely, Si and Mg in the Al lattice and consequently the formation of an Al-based supersaturated solid solution after 30 hours of milling. Earlier investigations [Chaubey et al. (2012) and Sivasankaran *et al*. (2010)] reported similar trend and attributed the variation in lattice parameter to the solute dissolution. The peak shift towards higher angles also indicates the existence of strain in the mechanically milled matrix [Zhao *et al.* (2005)]. The calculated and

experimental data for XRD patterns of Al are presented in Table 3.1. The unmilled powder has a lattice parameter of 4.0494 ± 0.0004Å, which is in agreement with the JCPDS No. 4-0787 data of pure Al. It is noted that the lattice parameter values of Al changes comparatively for 30 h of milling and is ascribed to the dissolution of alloying elements. In composite powders, during initial stages of milling, Al peaks shift towards lower angles due to the alloying elements which start to dissolve in Al matrix and at

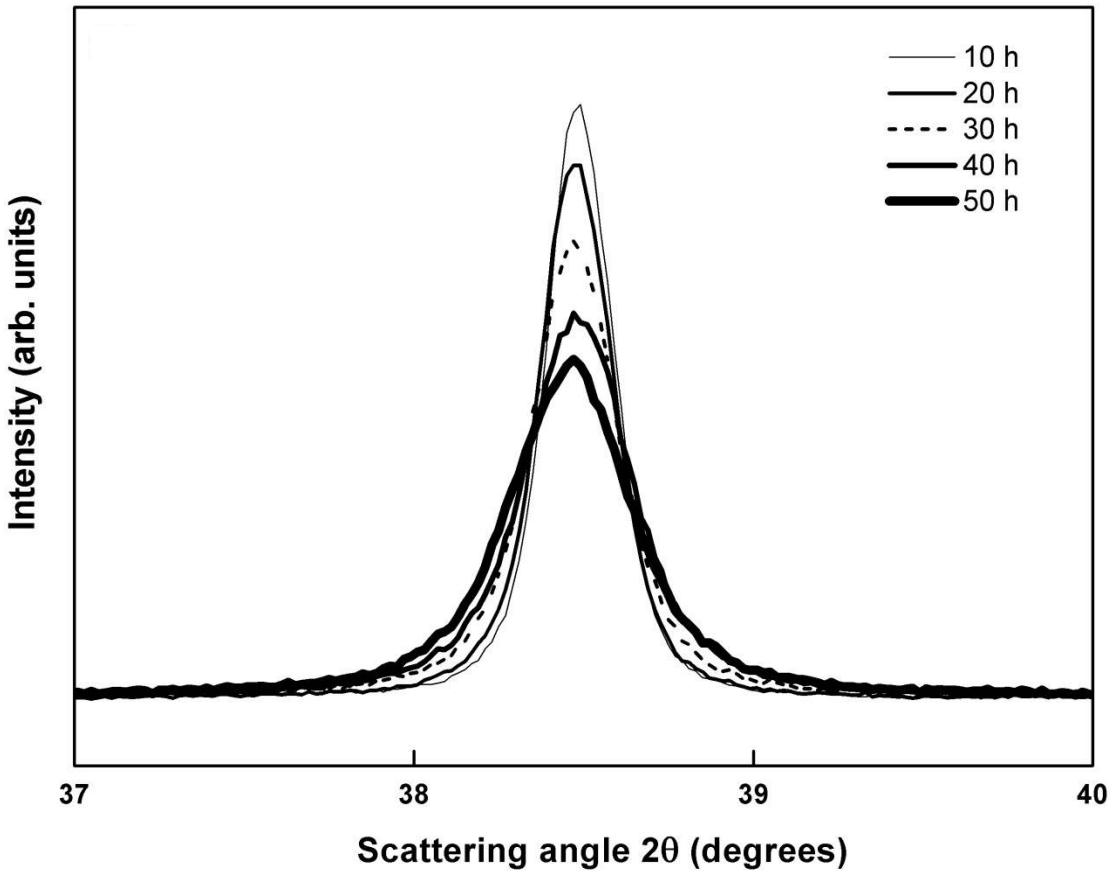

Figure 3.5: Evolution of d_{111} peak intensity on powder XRD showing the broadening and reduction in intensity milled at different hours for ENAW6082/Garnet.

Table 3.1: The calculated and experimental data for XRD patterns of un-milled to milled unreinforced EN AW6082.

hkl	$I/I_{max}(\%)$	$d_{cal}(\dot{A})$	$d_{exp}(\dot{A})$
0 h(a = 4.0494 Å)			
111	100	2.3379	2.3379
200	53	2.0247	2.0247
220	39	1.4316	1.4316
311	35	1.2209	1.2209
222	13	1.1689	1.1689
10 h(a = 4.0492 Å)			
111	100	2.3378	2.3379
200	50	2.0246	2.0247
220	37	1.4316	1.4317
311	34	1.2209	1.2209
222	11	1.1689	1.1690
20 h(a = 4.0492 Å)			
111	100	2.3378	2.3380
200	47	2.0246	2.0247
220	37	1.4316	1.4317
311	34	1.2209	1.2210
222	10	1.1689	1.1690
30 h(a = 4.0504Å)			
111	100	2.3385	2.3387
200	46	2.0252	2.0253
220	36	1.4320	1.4323
311	33	1.2212	1.2213
222	10	1.1692	1.1692
40 h(a = 4.0502 Å)			
111	100	2.3383	2.3386
200	45	2.0251	2.0254
220	35	1.4319	1.4322
311	32	1.2211	1.2213
222	10	1.1691	1.1691
50 h(a = 4.050 Å)			
111	100	2.3382	2.3384
200	46	2.0250	2.0251
220	35	1.4319	1.4319
311	33	1.2211	1.2214
222	10	1.1691	1.1692

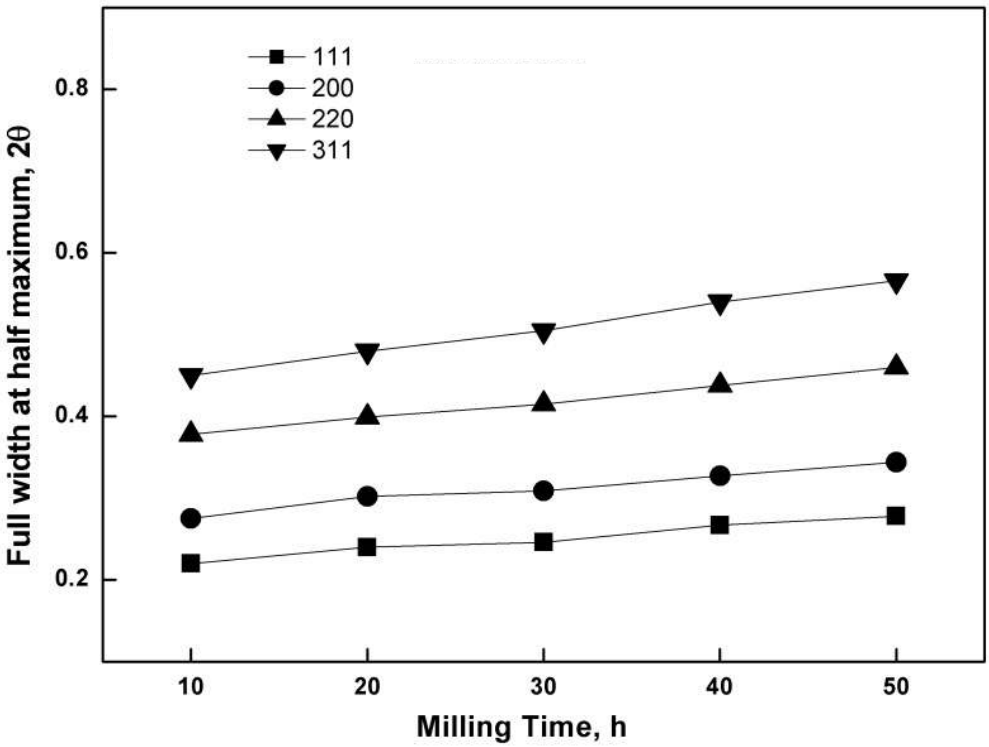

Figure 3.6: Full width at half maximum intensity of diffraction planes as a function of milling time for unreinforced EN AW6082.

later stages of milling no peak shifting was observed except for reduction in crystallite size due to interface structure, which has a large volume fraction in nanosize materials [Wang *et al*. (2001)]. The dissolution of alloying elements which causes peak displacement is also hindered by the hard rigid dispersoids and hence, in general, with garnet as reinforcement the peak shift is minimal.

X-ray line broadening, in terms of FWHM, with milling for unreinforced alloy and composites is shown in Figs. 3.6 through 3.8. It appears that the high energy milling increased the FWHM with increasing milling time and this may be ascribed to a severe lattice distortion and crystallite size refinement [Lonnberg (1994)]. During higher milling time the sample volume exhibiting small grains extends throughout the

entire specimen, hence decreasing the effective crystallite size [Fecht (1995)]. Figs. 3.9 through 3.11 show the variation of crystallite size and lattice strain with milling time for both the unreinforced as well as reinforced materials. It is clearly observed that the grain refinement in both Al/Garnet and EN AW6082/Garnet composites continued with increasing milling time due to presence of hard garnet particles and lattice distortion; and the large amount of lattice strain at final stages of milling is also due to the milling of hard reinforcement with the matrix materials. The crystallite size and microstrain of

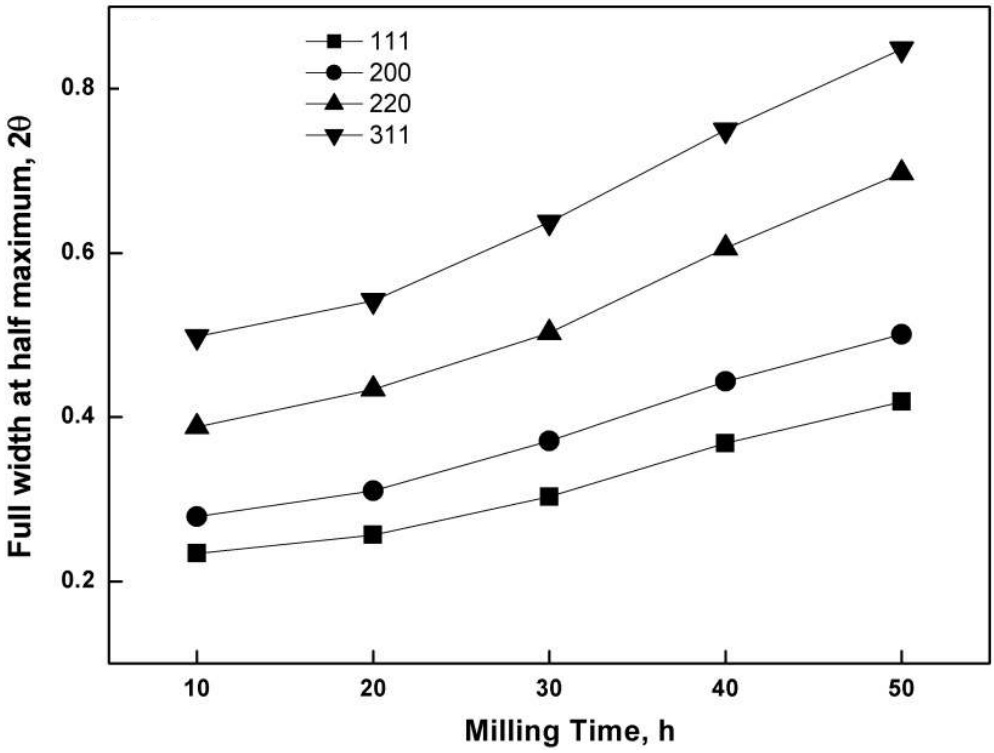

Figure 3.7: Full width at half maximum intensity of diffraction planes as a function of milling time for EN AW6082/Garnet.

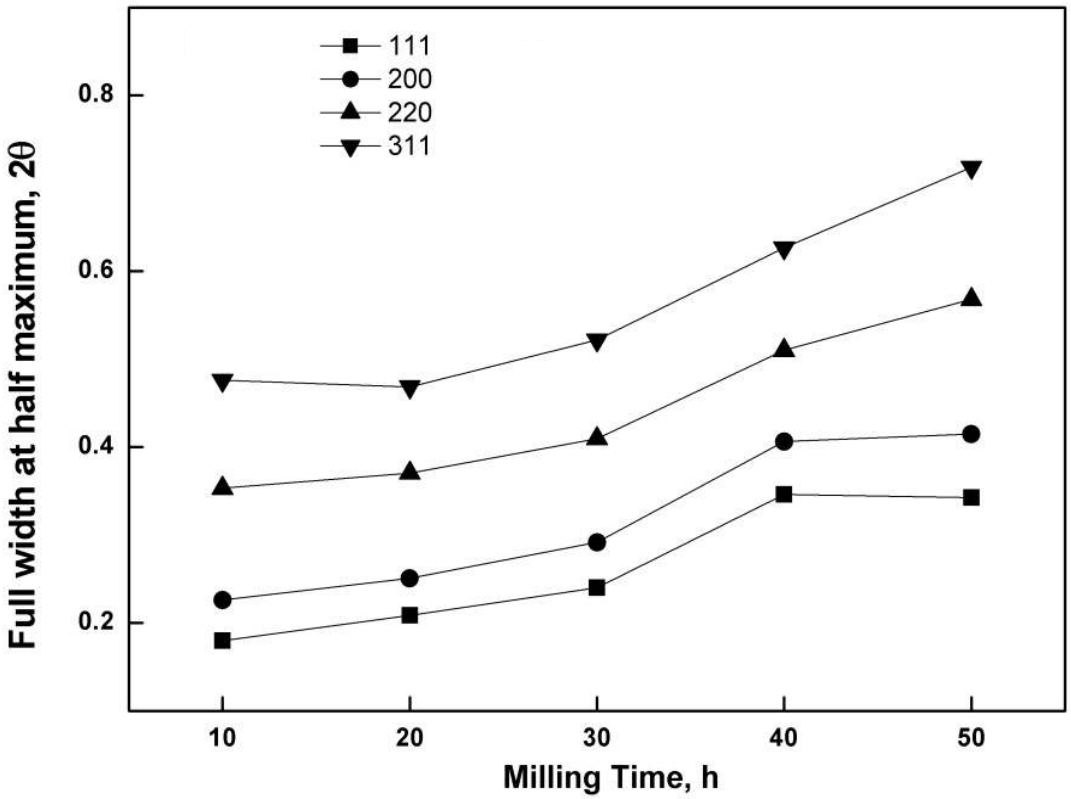

Figure 3.8: Full width at half maximum intensity of diffraction planes as a function of milling time for Al/Garnet.

Table 3.2: Mean crystallite size and apparent lattice distortion for powders after 10, 20, 30, 40 and 50 h of milling.

Material	Mean crystallite size (nm)					Apparent lattice distortion (%)				
	Milling time (h)									
	10	20	30	40	50	10	20	30	40	50
EN AW6082	119	110	69	56	54	0.187	0.215	0.219	0.237	0.260
EN AW6082/Garnet	153	96	68	48	36	0.229	0.248	0.283	0.323	0.369
Al/Garnet	419	373	148	79	42	0.233	0.237	0.238	0.244	0.312

the powders milled for 50 hours was determined using Williamson–Hall plots and are given in Table 3.2. The mean crystallite size calculated using Williamson–Hall plot was around 54, 36, and 42 nm for unreinforced EN AW6082, EN AW6082/Garnet, and Al/ Garnet, respectively, for a maximum milling time of 50 hours. The rate of refinement of the internal structure (crystallite size, lattice distortion, etc.) varies nearly logarithmically with milling time. Furthermore, addition of garnet particles makes the grain size still finer compared to unreinforced alloy. The milled EN AW6082 and hard reinforcement have resulted in greater microstructural refinement of about 36 nm

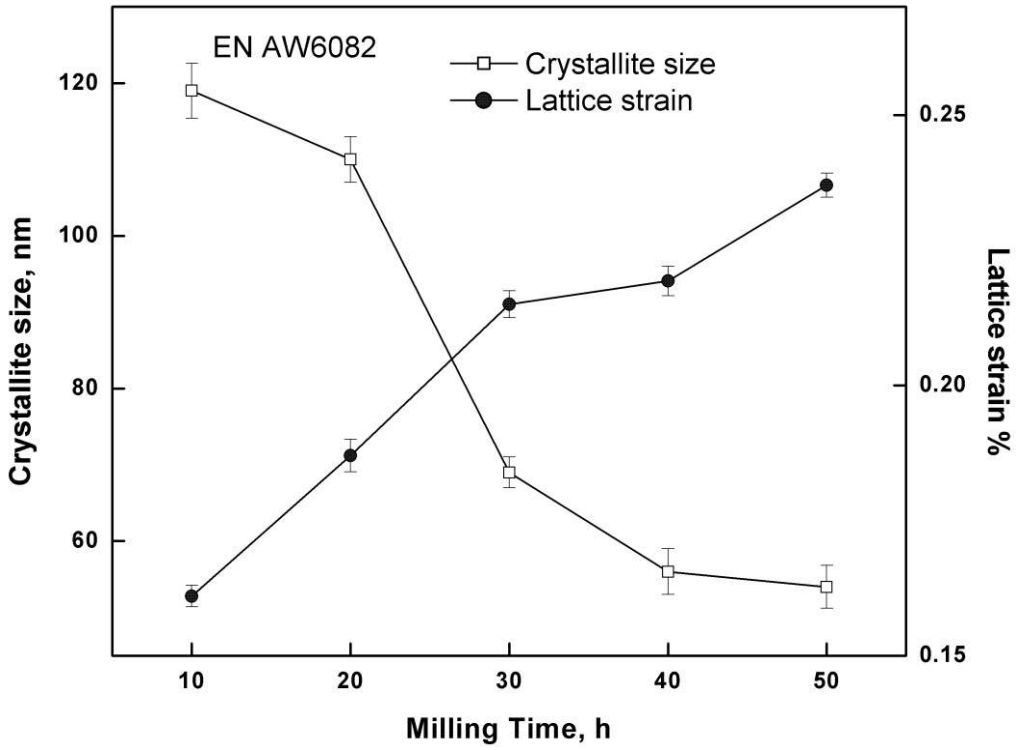

Figure 3.9: Variation in crystallite size and strain rate as a function of milling time for unreinforced EN AW6082.

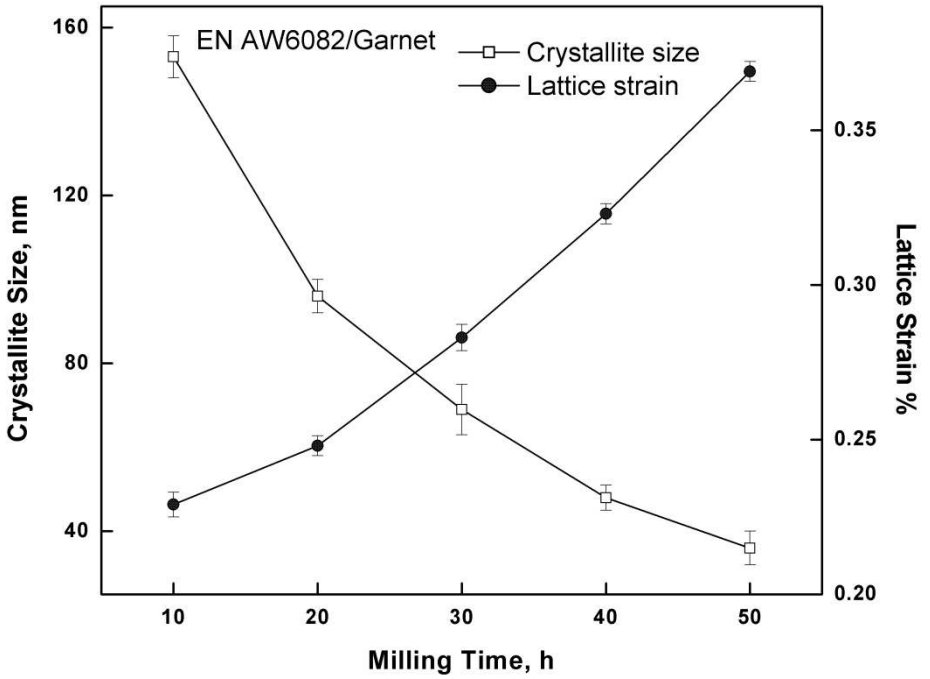

Figure 3.10: Variation in crystallite size and strain rate as a function of milling time for EN AW6082/Garnet.

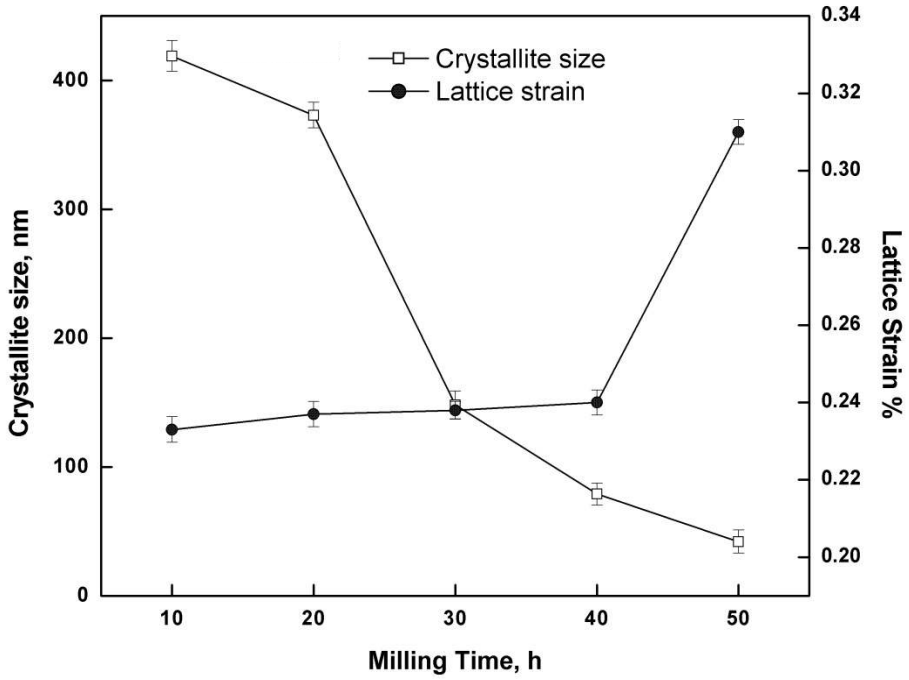

Figure 3.11: Variation in crystallite size and strain rate as a function of milling time for Al/Garnet.

compared to pure Al matrix with garnet. In the early stages of milling, a rapid decrease in crystallite size is observed due to the fact that the balls impart high impact force and transfers high kinetic energy to the particles which experience work hardening due to generation of a high dislocation density. However, the contribution of impact force to the grain refinement decreases with milling time due the fact that the increasing dislocation density lead to lower rate of plastic deformation as the milling progresses.

The reduction in rate of plastic deformation reduces the rate of dislocation generation and therefore gives rise to only small reduction in crystallite size and small increase in strain. These features were intensified in the composite powders because of the presence of hard garnet particles. In early stages of milling, severe plastic deformation of particles causes a deformed lattice with high density of dislocations. However, long milling time gives rise to nanocrystalline structure [Wang *et al*. (2001)]. The reduction in the Al grain size, in garnet reinforced particles, can be partially ascribed to the hindrance of the dislocation movement by Orowan strengthening mechanism. This results in increased dislocation density and thus accelerated grain refinement process. Lattice parameter of the composite mixture increases compared to unreinforced alloy due to addition of garnet particulates and grain refinement. With decreasing grain size, the volume fraction of grain boundaries increases and this results in pressure on the interfaces and tensile stress on the lattice and consequently leads to an increase in lattice parameter [Fecht (1995) and Qin *et al*. (1999)].

3.2 Particle size distribution

The PSD of the nano-composite powders milled for 50 hours is illustrated in Figs. 3.12(a) through (c). Table 3.3 presents D_{50} and D_{90} to D_{10} values related to the particle size of the composite samples. The D_{50} value represents the average particle

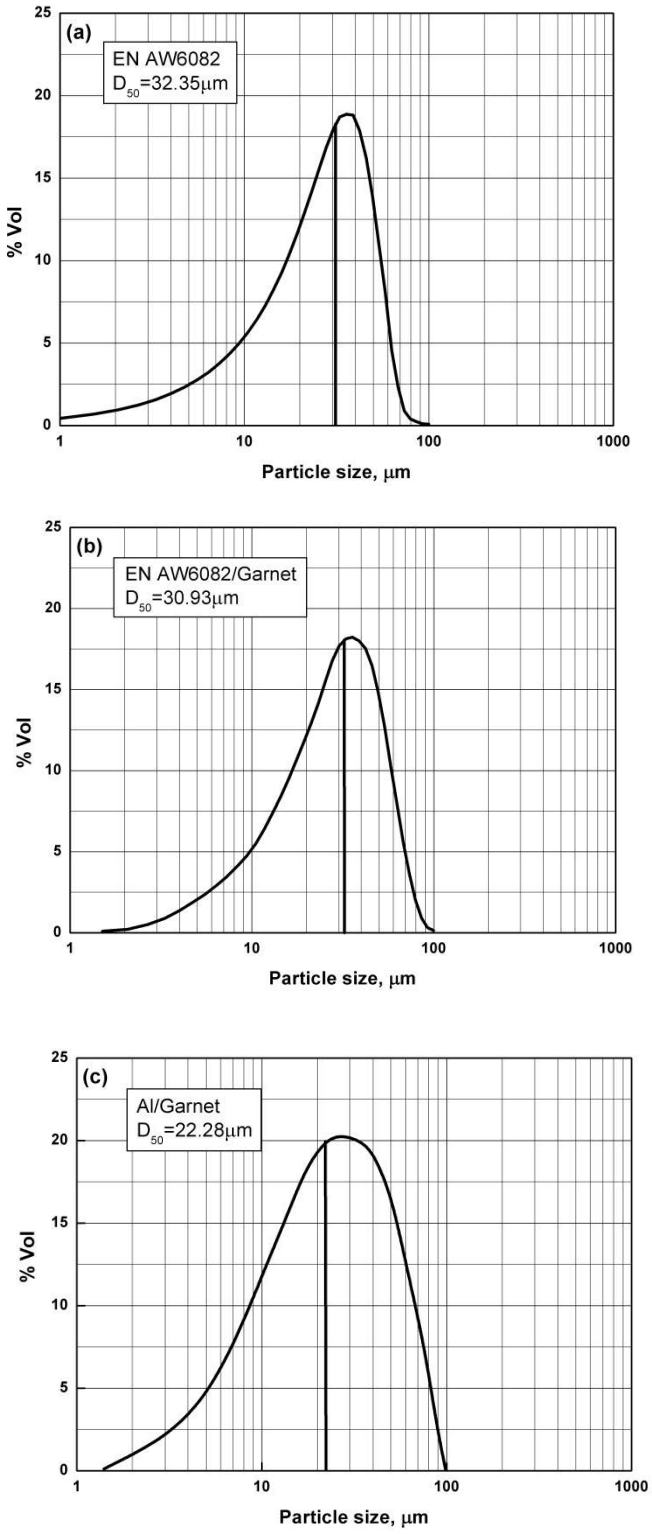

Figure 3.12: Particle size distribution of milled powders after 50 h (a) unreinforced EN AW6082, (b) ENAW6082/Garnet, and (c) Al/Garnet.

Table 3.3: Variation of characteristic diameters of powders after 50 h of milling.

Sample	Characteristic diameters (μm)	
	D_{50}	D_{90-10}
EN AW6082	32.35	93.36
EN AW6082/Garnet	30.93	80.57
Al/Garnet	22.28	35.12

diameter equivalent to 50 pct. of the particles undersize this value. The (D_{90} to D_{10}) is indicative of the spread of PSD. It is noticeable that all the milled powders exhibit relatively a lognormal size distribution. For unreinforced EN AW6082 (Fig. 3.12(a)), the PSD after 50 hours of milling shows an asymmetric behavior, which is indicative of the welding of matrix particles, and shows average particle size of 31 μm. During milling, fracture gives smaller range of particles and welding leads to larger range of particles and hence skewed distribution of the particles is obtained [Razavi *et al*. (2009)]. During MM process, cold welding and fracturing are the two main deformation mechanisms for ductile phase (Al and EN AW6082) and only fracture is possible for hard brittle garnet particles. The PSD of a material after grinding depends on the equilibrium between fracture and cold welding mechanisms [Delshad Chermahinia *et al*. (2009)]. Since hard materials are difficult to be abraded on their surfaces, the impact mechanism plays a dominant role and the brittle particles possess a greater tendency toward fracture rather than cold welding.[Fogognolo *et al*. (2003) and Razavi Hesabi *et al*. (2006)] Thus, the distribution curve of composite powders shows a symmetry and broader PSD, indicating the occurrence of equilibrium between fracture and welding—a typical steady state process, a characteristic of the final stage of MM.

Accordingly, the average particle diameter of the EN AW6082/Garnet composite powders was lower than that of unreinforced EN AW6082 powders.

3.3 Particle morphology and structure

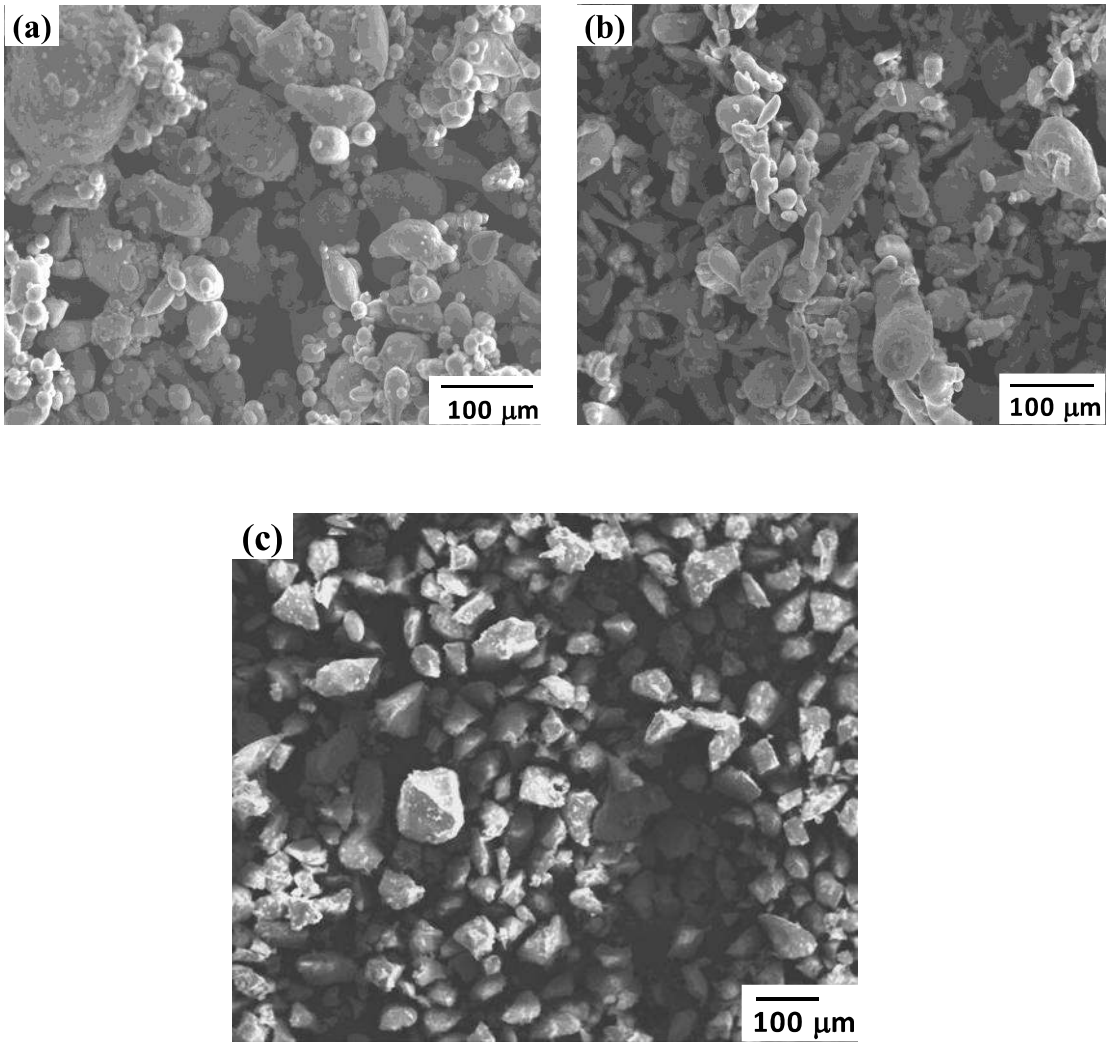

Figure 3.13: SEM micrographs of as-received powders (a) EN AW6082, (b) Pure Al and (c) Garnet.

The micrograph of as-received powder of EN AW6082 alloy shows almost a spherical morphology compared to pure Al, which revealed slightly elongated particle shape, as shown in Figs. 3.13(a) and (b). However, the EN AW6082 does show larger initial particle size. From Fig. 3.13(c) it is evident that the reinforcement particles are in the size range of 50 to 100 μm and have sharp edges and a faceted morphology. During ball milling, the blend of powder particles was first crushed under the impact of balls followed by cold welding process. Hence, the particle morphology changes from initial equiaxed to flattened shape due to initial pre-dominance of deformation. The final stage is characterized by the steady state process, in which the microstructural refinement occur and the morphology becomes once more equiaxed. The SEM of powders milled for 50 hours (Figs. 3.14(a), (b), and (e)), for all the powder mixtures, showed nearly equiaxed and finer particles indicating that the milling process has reached its steady state. Fig. 3.14(b) shows the SEM micrographs of powders milled for 50 hours and confirms the formation of layered microstructure and homogenous distribution of garnet particles in the soft aluminum matrix. Fig. 3.14(c) shows the high magnification SEM of EN AW6082/Garnet powder morphology after 50 hours, which reveals the reinforcement particles embedded on the surface of Al matrix as indicated by arrows. It also confirms the good interfacial integrity between aluminum matrix and garnet reinforcement. The corresponding EDS spectrum (Fig. 3.14(d)) reveals based on the particle composition, the presence of nanosized reinforcement particles in the Al matrix. Also, the Fig. 3.14(f) shows the magnified view of Al/Garnet composite particle revealing the entrapment of reinforcement particles into the soft matrix as indicated by arrows. From the present study of the morphology of particles, it is evident that the matrix powder has been severely deformed, with the garnet particles well dispersed into

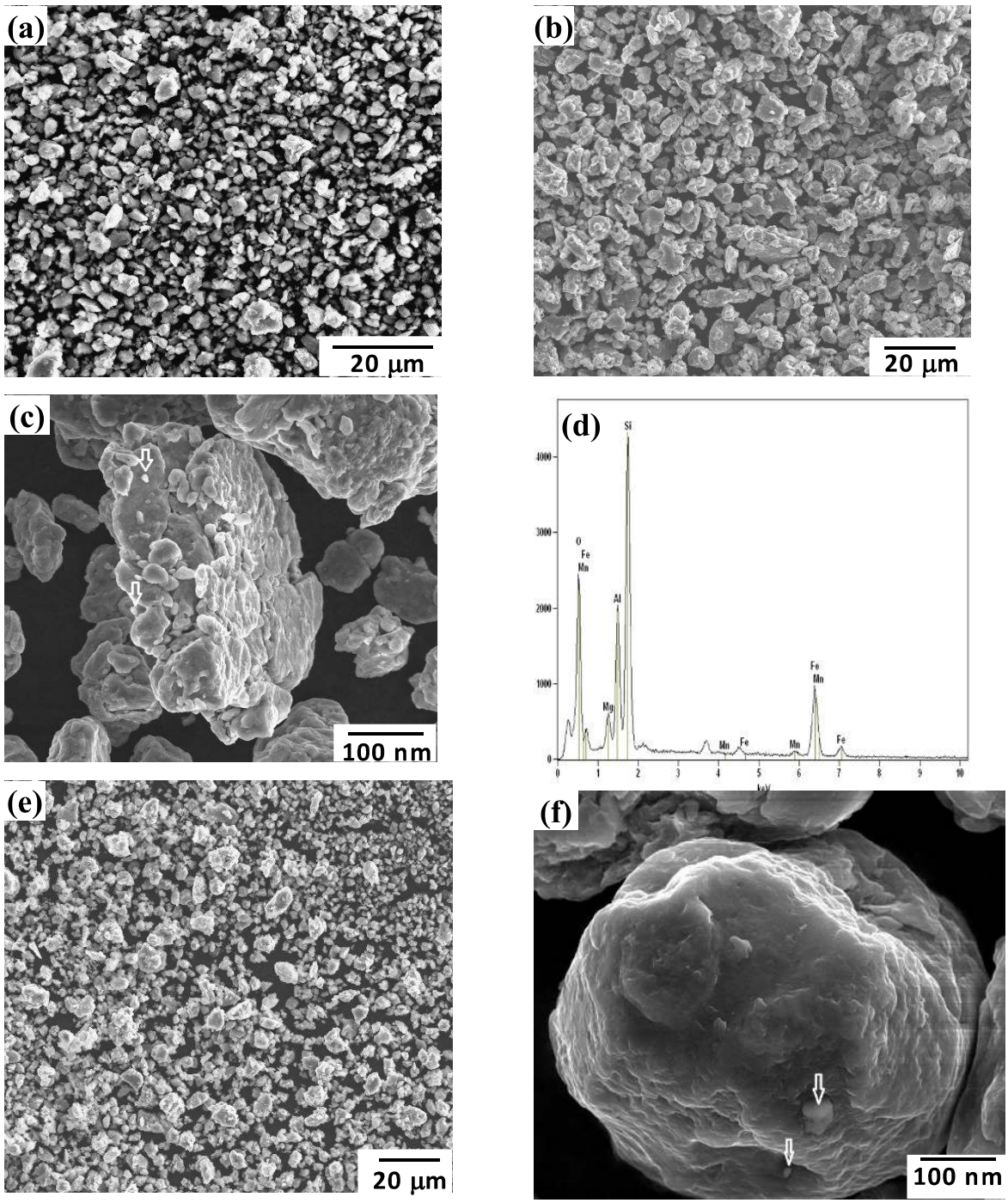

Figure 3.14: Morphology of milled powders for 50 h (a) unreinforced EN AW6082, (b) EN AW6082/Garnet, (c) Magnified view of EN AW6082/Garnet and (d) its corresponding EDS, (e) Pure Al/Garnet and (f) Magnified view of Pure Al/Garnet.

the matrix. The composite powders milled for 50 hours indicates the formation of clusters of fine particles and heavily deformed structure less than 50 nm in size. These findings are in good agreement with the crystallite size measurements made by XRD analysis.

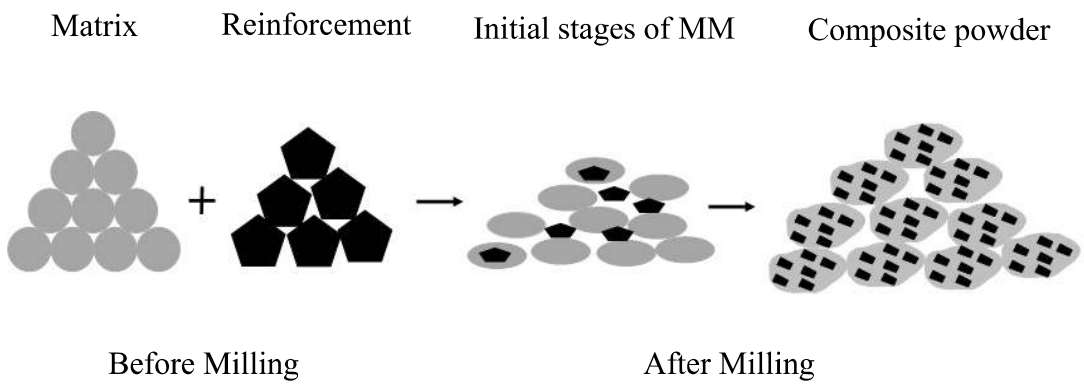

Figure 3.15: Schematic diagram proposing the formation of composite powder after high energy ball milling.

A possible scheme of the mechanical milling process for ductile matrix and brittle reinforcement has been proposed as shown in Fig. 3.15. In the very initial stage of milling, only a few garnet particles are incorporated into each of the Al-alloy particles. Then with further milling which causes work hardening of the Al-alloy and garnet phases, most of the garnet particles are deformed, fractured and incorporated into the Al-alloy matrix, forming Al-alloy/garnet composite powder particles as shown in Fig. 3.15. With continued milling, the garnet particles are reduced to nanometer sizes through continued fracturing. When the garnet particles reach a critical size, further fracturing becomes impossible during milling, and the composite microstrucutre stops changing. When the garnet particles are even smaller, perhaps < 36nm in diameter, it is

possible that the Al-alloy/Garnet surface energy is high enough to overcome the huge thermodynamic barrier to alloying Al-alloy and garnet. The garnet particles then lose their stability and dissolve into the Al-alloy matrix, forming Al-alloy (garnet) solid solution or Al-alloy-garnet amorphous alloy through mechanical alloying. Figs. 3.16(a) and (b) show the TEM micrographs of 50 hours milled EN AW6082 alloy powder. It reveals that the particles consist of equiaxed nanostructured grains with an average grain size of about 50 nm. The grain size measured from TEM micrographs is comparable with the crystallite size calculated from the XRD analysis, which yielded a value of 49 nm. The TEM micrographs of EN AW6082/Garnet and Al/Garnet composites are shown in Figs. 3.17 and 3.18, respectively. These micrographs confirm the nanocrystalline structure of the composite powders based on the extensive splitting

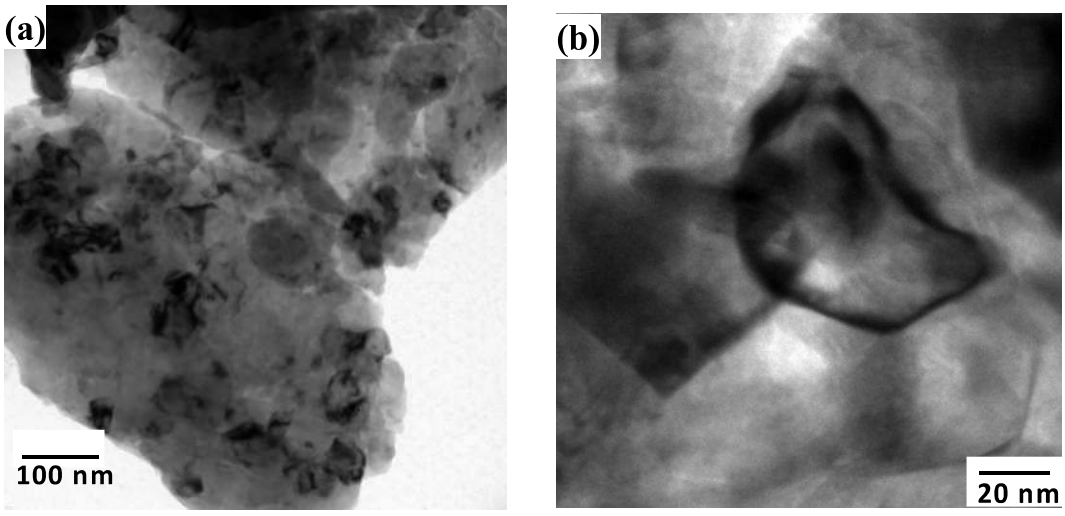

Figure 3.16: (a) TEM micrographs of 50 h mechanically milled powder particles of EN AW8082 alloy. (b) Magnified view of 'a'.

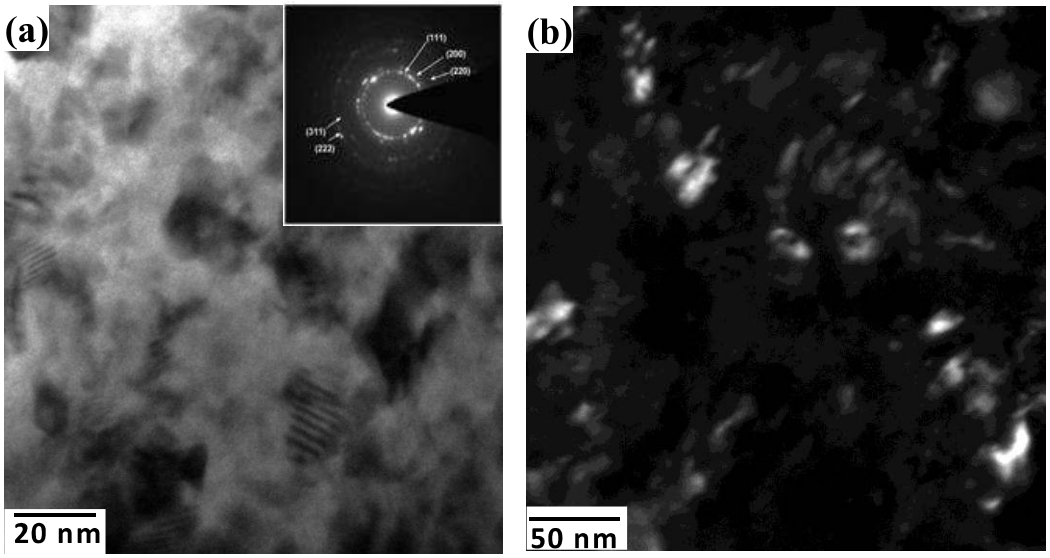

Figure 3.17: (a) TEM bright-field image of EN AW6082/Garnet MM for 50 h and its corresponding SAD pattern and (b) Dark-field image.

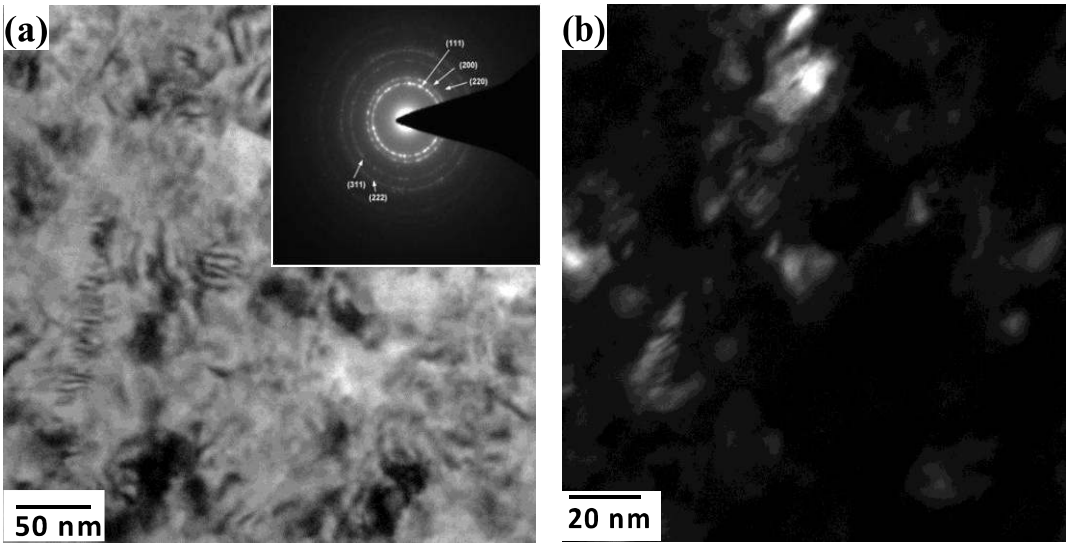

Figure 3.18: (a) TEM bright-field image of Al/Garnet MM for 50 h and its corresponding SAD pattern and (b) Dark-field image.

of the diffraction spots, as shown in the inset. The bright-field images (Figs. 3.17(a) and 3.17(a)) show that the two phases, namely garnet particles and aluminum matrix, are completely intermixed with each other. The dark-field images (Figs. 3.17(b) and 3.18(b)) clearly show deformed microstructure of grains of size less than 50 nm for both the composites. The selected area diffraction (SAD) patterns from the areas displayed in the bright field TEM images are shown as insets in Figs. 3.17(a) and 3.18(a) and the planes observed were assigned as (111), (200), (220), (311), and (222) of the Al matrix-FCC phase. The complex dislocation structures, a characteristic feature of a heavily deformed material, are evident in many areas. The contrast corresponds to microstructural defects such as shear bands that occur due to the high deformation rates during milling [Santos Beltran *et al*. (2006)]. These shear bands contain a high density of dislocations and precede the formation of substructure in the crystals and are more likely to contribute to increased hardness and reduced crystallite size.

3.4 Thermal analysis and structural stability

The differential thermal analysis (DTA) plots for all the 50 hours milled nanocrystalline powder samples are shown in Fig. 3.19. The DTA traces of all the peaks showed a sharp endothermic peak attributed to the melting of the matrix. The initial broad exothermic peak can be due to the evaporation of moisture present in the powders or some other extraneous effects. The second exothermic peak observed in the temperature range of 473 K to 773 K (200^{o}C to 500^{o}C) in the case of EN AW6082, as depicted in Fig. 3.19, was due to the dissolution of all the precipitates into the aluminum matrix, which formed a diffusion couple with an increased ball milling time [Woo *et al*. (2006)]. The melting temperature obtained using thermal analysis was

around 924 K, 925 K, and 928 K (651°C, 652°C, and 655°C) for unreinforced EN AW6082, EN AW6082/Garnet, and Al/Garnet, respectively. This slight decrease in the melting point of unreinforced EN AW6082 is attributed to mechanical alloying of the powder particles which increases the surface area of the particles and surface energy of the nanocrystalline powders, when compared to other milled powders. It is also known

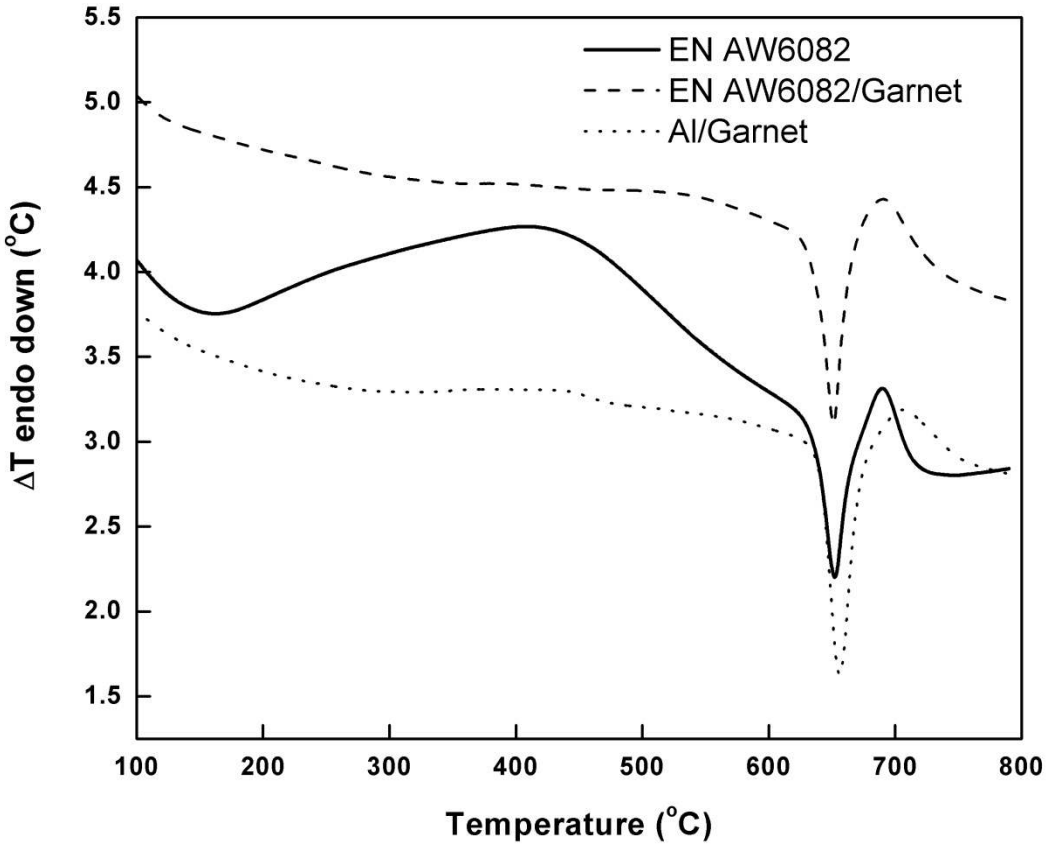

Figure 3.19: DTA curves of milled powders for 50 h of unreinforced EN AW6082, EN AW6082/Garnet and Al/Garnet.

from phase diagrams theory that when a solid solution is formed, it has a lower melting point compared with the starting pure elements [Hemandez *et al*. (2010)]. The addition of reinforcement particles in the aluminum matrix has significantly altered the nature of

DTA traces observed in comparison to unreinforced EN AW6082 alloy powder. The broad exothermic peak from 373 K to 804 K (100^{o}C to 531^{o}C) in EN AW6082/Garnet, and 373 K to 811 K (100^{o}C to 538^{o}C) in Al/Garnet powder mixture occurred over a period of time may be attributed to strain release and grain growth [Azabou *et al*. (2009) and Maiti *et al*. (2008)].

3.5 Hardness variation

The microhardness variation with milling time for unreinforced alloy and composite powder is shown in Fig. 3.20. It is evident from the plot that both unreinforced alloy and composite powder show increasing hardness with milling time. The hardness of the Al/ Garnet did not increase much up to 20 hours of milling. The slower rate of increase

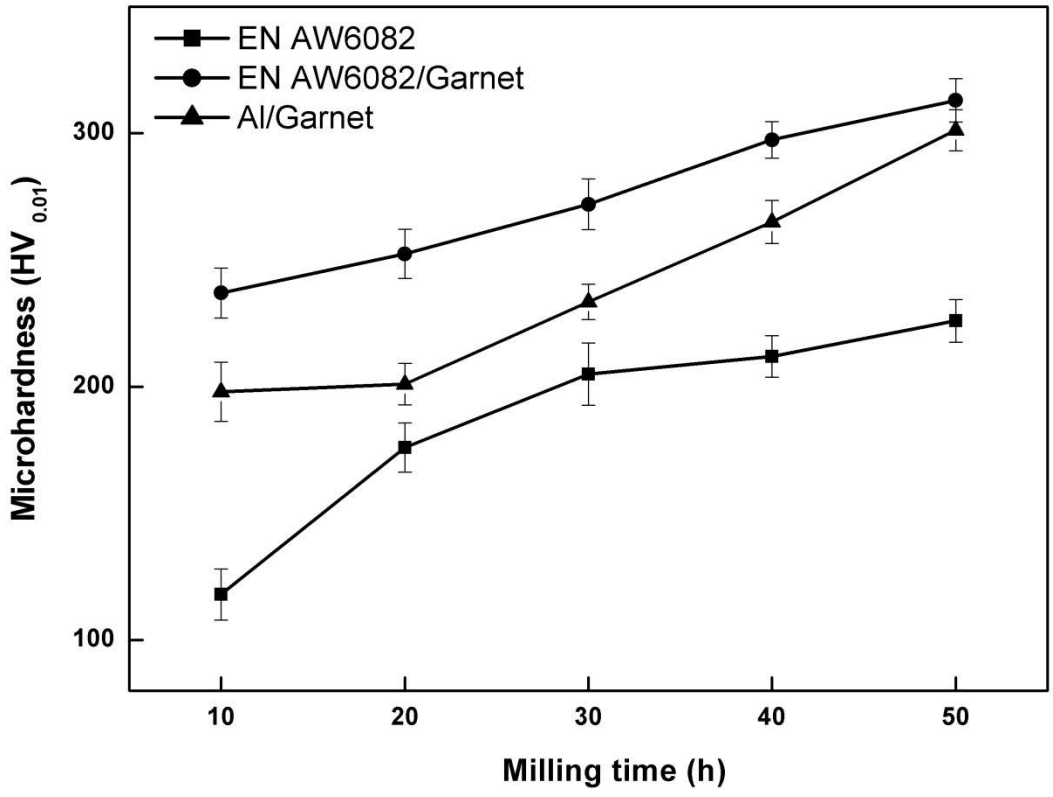

Figure 3.20: Powder hardness as a function of milling time for different systems.

in microhardness may be attributed to the dynamic recovery caused by high work hardening effects of deformed matrix and static recovery of highly deformed matrix with local increase of temperature in particles during collisions [Safari *et al*. (2011)]. However, the hardness of both the composites reached closer to each other after 50 hours of milling viz. 313 HV for EN AW6082/Garnet and 301 HV for Al/Garnet. These values are higher in comparison with initial hardness data of pure aluminum and aluminum alloy whose values are about 71 HV and 75 HV, respectively. The hardening of the milled powder has been shown to be influenced by the combination of several factors: (1) lattice strain, which increases as a result of deformation during ball milling and introduces a large density of dislocation. The dislocation density contributes to the strength of the material and can be calculated on the basis of the Taylor equation [Ashby (1970)], (2) dispersion hardening, which can be estimated using the Orowan strengthening mechanism [Brown *et al*. (1971)], and (3) grain size, which is the most important factor and can be explained by the Hall–Petch relationship. The highest microhardness values are attained for EN AW6082/Garnet composite powders. The significant increase in hardness with garnet reinforcement particles can be attributed primarily to: (a) the presence of relatively harder particulates in the matrix, (b) a higher constraint to the localized matrix deformation during indentation due to their presence, (c) reduced grain size, and (d) no possibility of cluster formation [Fogognolo *et al*. (2003)]. To verify the relationship between microhardness and grain size, a combination of classical Hall–Petch equation [Hall (1951) and Petch (1953)] and Tabors empirical relationship [Tabor (1951)], $H = 3\sigma$ is used. It is known that the strength varies according to the following semi-empirical Hall–Petch equation as given

in equation 1.6. Figs. 3.21(a) through (c) show the H–P plot of microhardness (HV0.01) vs inverse root of grain size for milled unreinforced EN AW6082, reinforced EN AW6082 and reinforced Al composite powders, respectively. A linear fit to the experimental results of the hardness values (VHN) against the inverse of the square root of the grain ($d^{-1/2}$) revealed the value of H_0, K and correlation coefficient as presented in Table 3.4. These values are higher than mechanically milled nanocrystalline pure aluminum powders reported by Hamid Abdoli *et al.* (2011) which revealed value of 7.3 ± 2 MPa and 373 ± 75 $(nm)^{1/2}MPa$ for H_0 and K, respectively, confirming that the influence of reinforcement type, size and alloying element has greater impact on the

Table 3.4: Fitting constants obtained from Hall-Petch equation.

System	$H_0(MPa)$	$K(nm)^{1/2}$	R^2
EN AW6082	32.5±14	756.43±140	0.998
EN AW6082/Garnet	54.6±10	298.72±80	0.997
Al/Garnet	50.3±6.7	328.25±68	0.997

mechanical properties of the composite powders. The slope of the linear fit in all the systems is positive and hence it can be evidenced that the above relationship holds good for the present investigation; and further the higher slope can be attributed to high density of dislocations generated during high-energy milling [Sato *et al*. (2003)]. The strengthening effect in particulate-reinforced metal matrix composites is attributed to three main factors involving: (i) Orowan strengthening effect, (ii) enhanced dislocation density due to the residual plastic strain caused by the difference in the coefficients of thermal expansion between the matrix and particles, and (iii) load-bearing effect of the hard reinforcements [Zhang *et al*. (2006)]. Zhang and Chen (2007) have proposed an

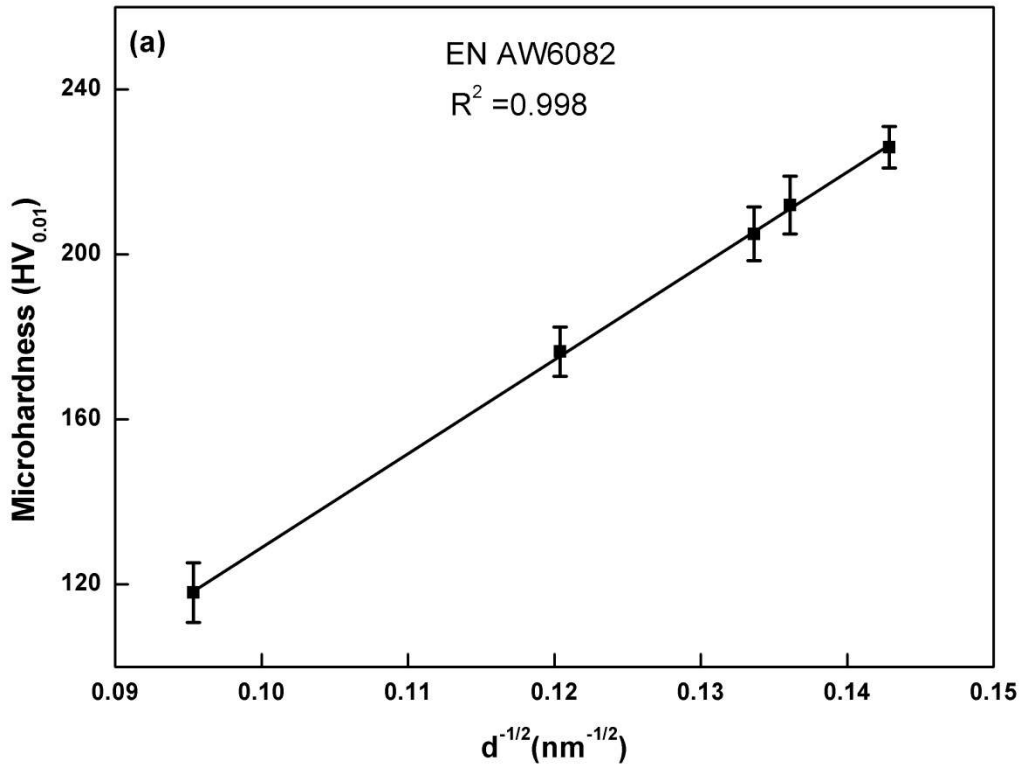
(a)
EN AW6082
R2 =0.998
Microhardness (HV0.01)
240
200
160
120
0.09
0.10
0.11
0.12
0.13
0.14
0.15
d-1/2(nm-1/2)

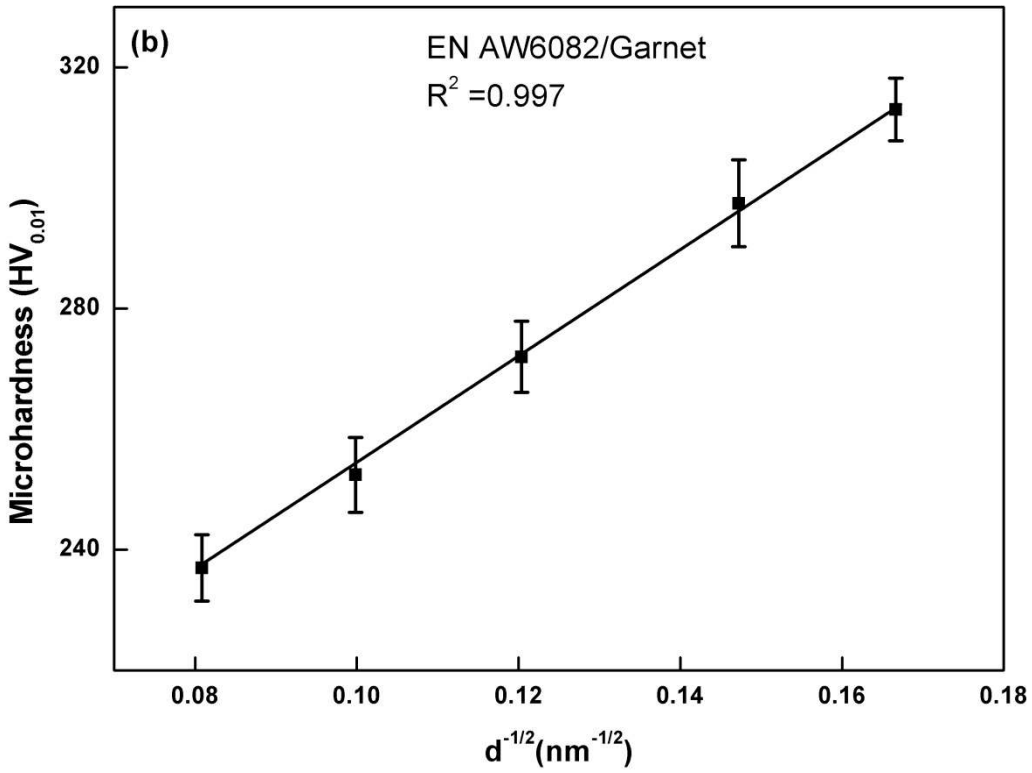
(b)
EN AW6082/Garnet
R2 =0.997
Microhardness (HV0.01)
320
280
240
0.08
0.10
0.12
0.14
0.16
0.18
d-1/2(nm-1/2)

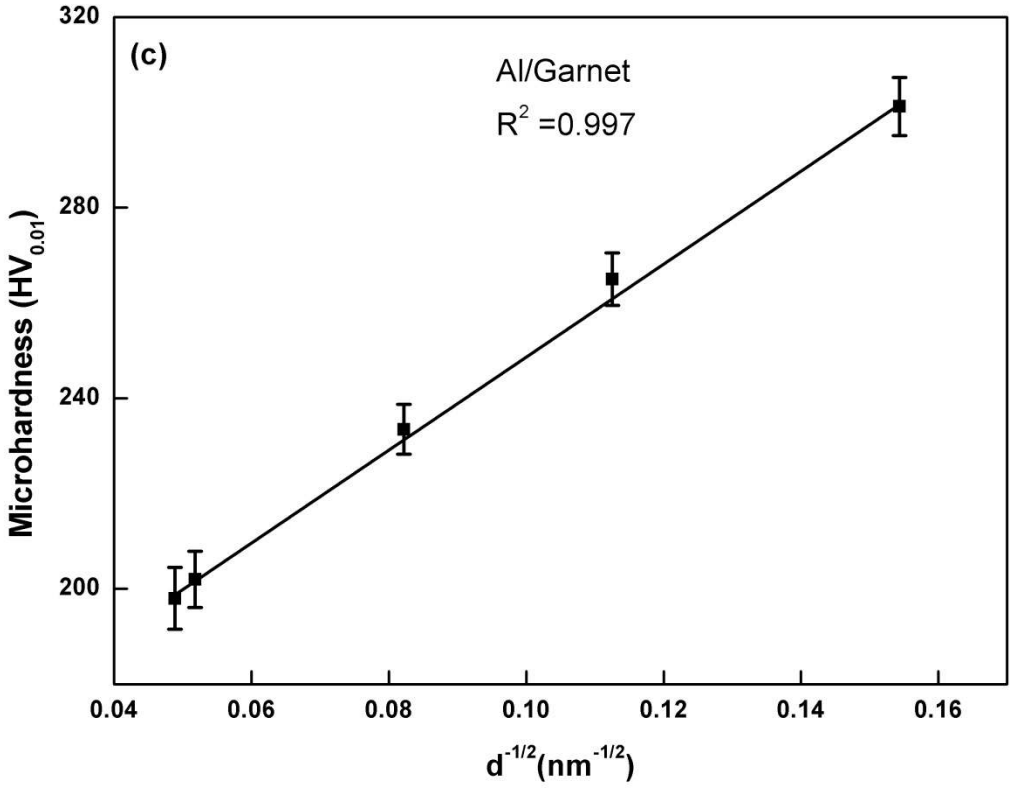

Figure 3.21: Hardness of milled powders as a function of grain size (a) unreinforced EN AW6082, (b) EN AW6082/Garnet and (c) Al/Garnet.

analytical expression to predict the yield strength by incorporating the three effects mentioned above as given by the equations 1.1.

The model proposed by Zhang and Chen (2007) was used to understand the strengthening effect of the ball-milled composite in the present study. In addition, similar strengthening model proposed by Ramakrishnan (1996), which does not take into account the Orowan strengthening effect (Orowan), was also considered. Using Tabor relation [Tabor (1951)], hardness is assumed to correspond to the yield stress

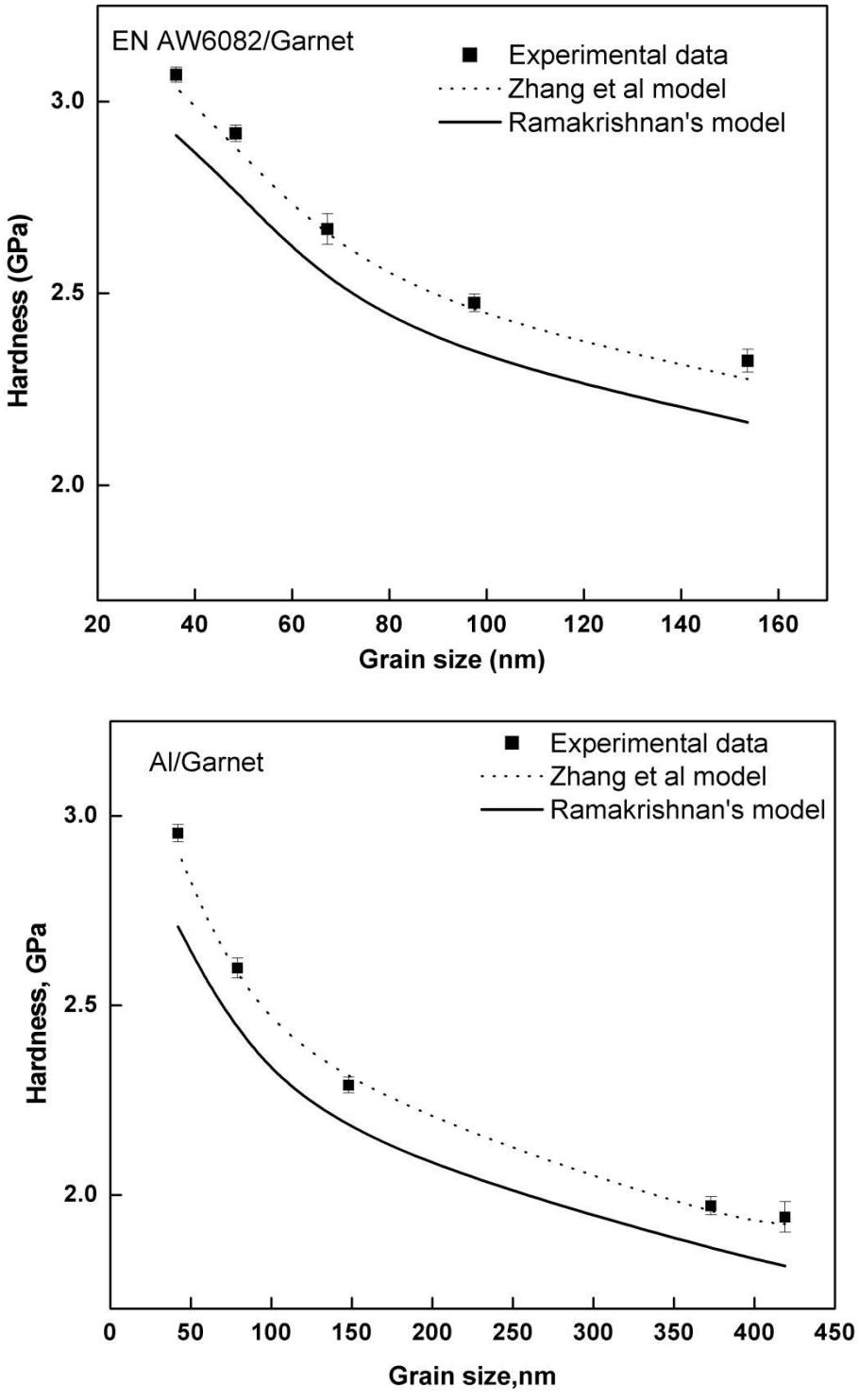

Figure 3.22: Comparison of the model predictions via varying grain size with the experimental data for EN AW6082 and Al composite.

multiplied by a factor of three. Fig. 3.22 shows the hardness predicted by the Zhang model, i.e., by equation. 1.1, and Ramakrishna model in a garnet particulate reinforced Al and EN AW6082 Al-alloy composite. The validity of the equation was checked against available experimental data and a reasonable agreement was observed with the values predicted by the model proposed by Zhang *et al*., as shown in Fig. 3.22. The accuracy of the estimation of hardness using model was well within an order of magnitude. This indicates that the calculations based on the strengthening mechanisms involving combined effect of load bearing, dislocation strengthening and Orowan strengthening can be used to accurately model the hardness of the present ball-milled particulate-reinforced composites.

3.5.1 Nanohardness measurement

The typical load–displacement curves for 50 hours milled unreinforced alloy and composite powders are shown in Fig. 3.23. The curves are for the indentations made to peak load of 100 mN at room temperature and exhibit typical elastic behavior. The differences in hardness of the milled powders are apparent from the large differences in peak depth. The elastic modulus and hardness, estimated from this curve, are given in Table 3.5. All the hardness and the elastic modulus values obtained are higher than that for pure aluminum, which has a hardness value of 0.7 GPa [Mondolfo

Table 3.5: Elastic modulus and hardness of the unreinforced alloy and composite constituents MM for 50 h measured by nanoindentation.

System	E (GPa)	H (GPa)
EN AW6082	104 ± 12	3.02 ± 0.4
EN AW6082/Garnet	148 ± 7	4.24 ± 0.07
Al/Garnet	127 ± 9	3.63 ± 0.1

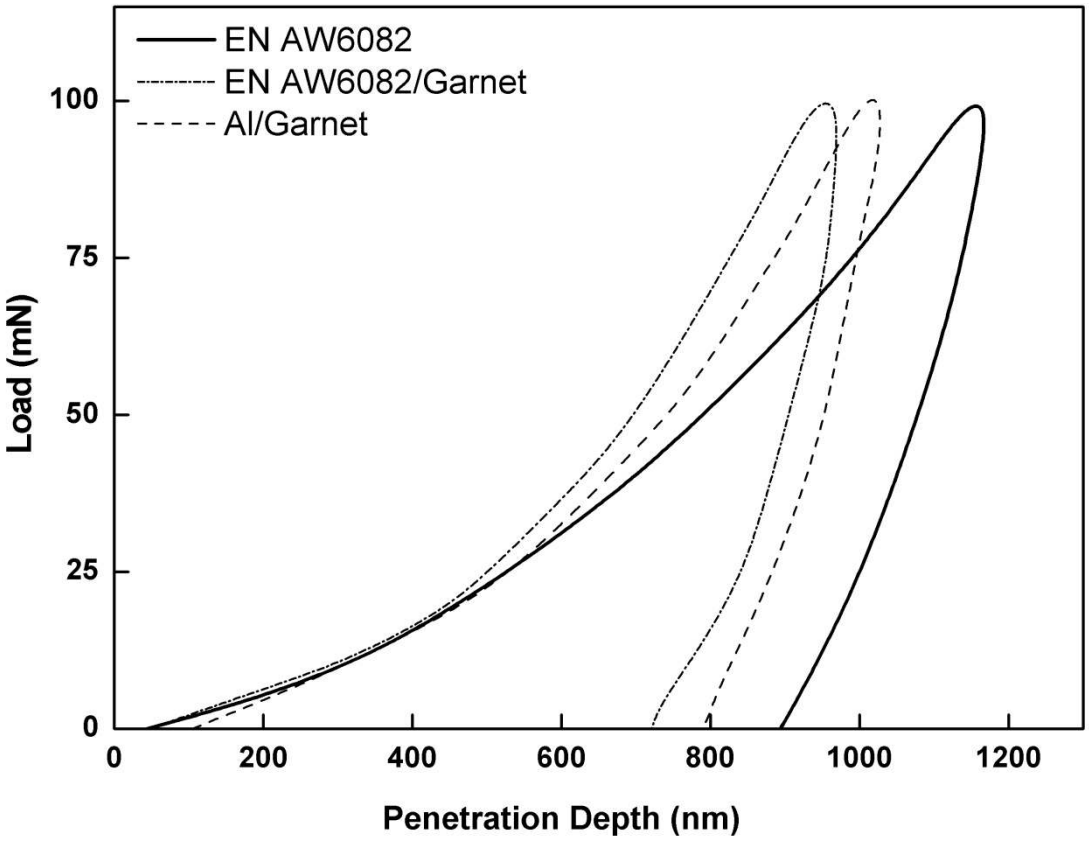

Figure 3.23: Load versus penetration depth curves of unreinforced EN AW6082 and composite powders milled for 50 h.

(1976)] and elastic modulus of 76 GPa [Nayak *et al.* (2004)]. Hence, parameters such as high-energy ball millig, addition of reinforcement and alloying elements has considerably increased the hardness values almost 4.3, 6.0, and 5.2 times for unreinforced and reinforced alloy and Al/garnet composite, respectively, compared to pure aluminum. Orowan strengthening, grain size and substructure strengthening, quench hardening resulting from the dislocations generated to accommodate the differential thermal contraction between the reinforcing particles and matrix, and work

hardening due to the strain misfit between the elastic reinforcing particles and the particle matrix [Miracle (2005)] are the possible strengthening mechanisms which may operate simultaneously leading to increased hardness and elastic modulus. Difference in microhardness and nanohardness of milled powders could be due to indentation size effect (ISE) [Mukhopadhyay *et al*. (2006)]. Nanoindendation results show that the addition of garnet in EN AW6082 matrix increased the hardness and elastic modulus from 3.02 and 104 GPa to 4.24 and 148 GPa, respectively, after 50 hours of milling. With increase in milling time, the reinforcement particle size decreases, which have a positive effect on the mechanical properties of the composite powders.

3.6 Conclusions

The influence of high-energy ball milling time on the morphological and structural features, lattice strain, crystallite size and mechanical properties of unreinforced and garnet reinforced EN AW6082 alloy and garnet reinforced pure Al powders has been investigated. The results of the above investigation have led to the following conclusions:

(1) High-energy milling method, used for the preparation of composite powders with hard particle reinforcement resulted in refined microstructure and randomly oriented interfacial grain boundaries.

(2) XRD evaluation did not indicate any phase transformation during milling of unreinforced EN AW6082, EN AW6082/Garnet, and Al/Garnet composite blends. However, α-Al peaks evidenced a shift in their original position. Intense effect was observed in unreinforced EN AW6082 alloy due to formation of

supersaturated solid solution, contrary to other composite mixture where the peak shift is minimal due to presence of hard dispersoids.

(3) The crystallite size of the aluminum alloy in the composite powder was smaller than that of the unreinforced alloy at the same milling time and the size reached to 36 nm for EN AW6082/Garnet after 50 hours milling.

(4) Among the different composites investigated, EN AW6082/Garnet was found to be most effective in microstructural refinement and improved mechanical properties. The variation of hardness values with grain size follows the empirical Hall–Petch relationship.

(5) Strengthening model prediction involving Orowan effect was found to be in agreement with the experimental data for both Al and Al-alloy composites synthesized by high-energy milling.